Available online at www.sciencedirect.com
SCIENCE DIRECT
Journal of Magnetic Resonance 181 (2006) 68–78
JMR Journal of Magnetic Resonance
www.elsevier.com/locate/jmr

Fast amplitude-modulated pulse trains with frequency sweep (SW-FAM) in static NMR of half-integer spin quadrupolar nuclei

Thomas Bräuniger [a,*], Günter Hempel [a], P.K. Madhu [b]

[a] Department of Physics, University of Halle, Friedemann-Bach-Platz 6, 06108 Halle, Germany
[b] Department of Chemical Sciences, Tata Institute of Fundamental Research, Homi Bhabha Road, Colaba, Mumbai 400 005, India

Received 5 February 2006; revised 20 March 2006
Available online 17 April 2006

Abstract

In solid-state NMR of quadrupolar nuclei with half-integer spin I, fast amplitude-modulated (FAM) pulse trains have been utilised to enhance the intensity of the central-transition signal, by transferring spin population from the satellite transitions. In this paper, the signal-enhancement performance of the recently introduced SW-FAM pulse train with swept modulation frequency [T. Bräuniger, K. Ramaswamy, P.K. Madhu, Enhancement of the central-transition signal in static and magic-angle-spinning NMR of quadrupolar nuclei by frequency-swept fast amplitude-modulated pulses, Chem. Phys. Lett. 383 (2004) 403–410] is explored in more detail for static spectra. It is shown that by sweeping the modulation frequencies linearly over the pulse pairs (SW($1/\tau$)-FAM), the shape of the frequency distribution is improved in comparison to the original pulse scheme (SW(τ)-FAM). For static spectra of ^{27}Al ($I = 5/2$), better signal-enhancement performance is found for the SW($1/\tau$)-FAM sequence, as demonstrated both by experiments and numerical simulations.
© 2006 Elsevier Inc. All rights reserved.

Keywords: Static ^{27}Al NMR; Half-integer spin; Quadrupolar nuclei; SW-FAM

1. Introduction

Half-integer spin quadrupolar nuclei constitute the majority of spins observable by NMR spectroscopy in technologically important materials such as minerals, ceramics, catalysts and glasses [1], e.g., ^{7}Li, ^{11}B, ^{23}Na with $I = 3/2$, and ^{17}O, ^{25}Mg, ^{27}Al with $I = 5/2$. In most cases, solid-state NMR characterisation of inorganic materials is restricted to observing the position and shape of the second-order quadrupolar broadened central-transition peak. However, even with magic-angle-spinning (MAS) [2] for partial averaging of the second-order broadening of the spectral lines, sensitivity problems persist for numerous nuclei, caused by small gyromagnetic ratios, low natural abundance, strong quadrupolar interaction or by any combination of these factors. These problems become even more pronounced if static spectra need to be acquired [3,4].

Recently, there has been a renewed interest in the enhancement of the central-transition signal of nuclei by using spin population transfer techniques. In 1981, Vega and Naor [5] described the idea of enhancing the signal of the central transition by re-arranging the populations of the spin levels in such a way that the population difference of the $m = -1/2 \rightarrow +1/2$ transition is increased prior to the read pulse. As can be seen from Fig. 1A, complete inversion of the satellite transitions of a half-integer spin I leads to an enhancement of the central-transition intensity by a factor of $2I$, while complete saturation of the satellite transitions results in an improvement factor of $I + 1/2$. Several experimental approaches were suggested to realise the desired signal enhancement. In 1993, Haase et al. [6–8] used especially adapted probe circuits (“dual-Q probe”) and applied frequency-swept adiabatic passages for transfer of spin population from the outer spin levels to the central transition. The predicted intensity increase

* Corresponding author. Fax: +49 345 5527161.
E-mail address: thomas.braeuniger@physik.uni-halle.de (T. Bräuniger).

1090-7807/$ - see front matter © 2006 Elsevier Inc. All rights reserved.
doi:10.1016/j.jmr.2006.03.016

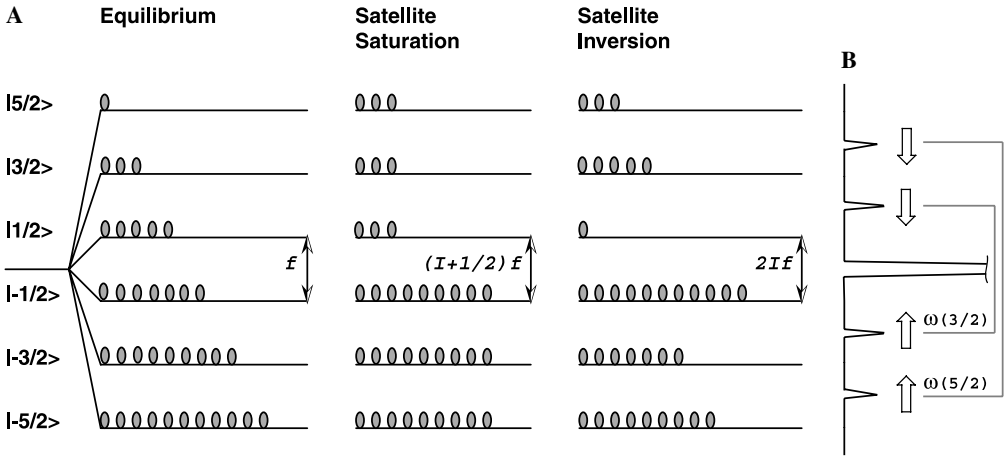

Fig. 1. (A) Schematic (exaggerated) spin population distribution for an $I = 5/2$ nucleus in an external magnetic field. The spectral intensity for the central transition ($m = -1/2 \rightarrow +1/2$) is proportional to the population difference f. In the case of saturation of the satellite transitions, the achieved enhancement factor for the central-transition signal is $(I + 1/2)$, while for selective inversion of the satellite transitions (progressing from the outer to the inner ones), the enhancement factor is $2I$. (B) Schematic representation of a single-crystal NMR spectrum of an $I = 5/2$ nucleus, with central-transition and satellite-transition peaks. For manipulation of the spin level populations, the frequencies of the applied RF modulations need to be matched to the positions of the satellite peaks, $\omega(3/2)$ and $\omega(5/2)$. The arrows indicate the direction of the frequency sweep applied in DFS [9] and SW-FAM [22].

of the central-transition signal was thus demonstrated for several quadrupolar nuclei, e.g., ^{27}Al [6,7] and ^{17}O [8]. In a series of articles, starting in 1998, Kentgens and co-workers [9–13] have explored the applicability of double-frequency sweeps (DFS) for spin population transfer. Here, the satellite transitions are traversed by an amplitude modulation of the RF carrier of appropriate frequency, and enhancement factors up to the theoretical maximum were achieved [13]. Also, the principle of using hyperbolic secant pulses for selective inversion [14] has recently been applied to half-integer spin quadrupolar nuclei by Wasylishen and co-workers [15] with very convincing results for static ^{23}Na spectra of single crystals and ^{87}Rb MAS spectra of powder samples.

An alternative approach is the use of fast amplitude-modulated (FAM) pulses, which have also been employed for signal enhancement in multiple-quantum (MQ) NMR [5,16,17]. A FAM pulse train consists of a series of radio-frequency (RF) pulses of uniform duration, with a 180° phase shift between consecutive pulses. Thus, an amplitude modulation of a certain frequency is approximated using standard RF pulses, which are straightforward to produce on NMR spectrometers, without the need for additional hardware or pulse shaping tools. The use of FAM-type pulse trains for saturating the satellite transitions of polycrystalline (powder) samples under MAS has been demonstrated by Grandinetti and co-workers [18]. This work was later extended to include Gaussian pulse trains [19], and multiple-passage schemes for additional signal enhancement [20]. For a single crystal spectrum, $(I - 1/2)$ FAM trains with decreasing modulation frequencies are needed to traverse all satellite transitions of a nucleus with half-integer spin I, as shown in Fig. 1B. Therefore, one FAM train with a single modulation frequency is sufficient for re-arrangement of the spin level populations for a spin-3/2 nucleus [18]. The best signal enhancement for spin-5/2 nuclei is achieved by using two modulation frequencies, to consecutively affect the outer and inner satellite transitions [21]. In theory, matters get more complex for the usually encountered case of powder samples, where the RF effects on the spins are varying with the respective orientation of the crystallites. In practice, all spin population transfer techniques described above, including FAM, work remarkably well for MAS spectra of powdered samples, without introducing appreciable line shape distortions. Partly, this can be attributed to a population transfer process via adiabatic level crossings induced by the sample rotation (the acronym RAPT [18–20], 'rotor assisted population transfer,' refers to this process). Enhancement of static spectra is also possible, but more difficult to attain, because no MAS-induced level crossings occur, and the population transfer is caused solely by the RF modulation.

To improve the performance of FAM pulse trains for static spectra, and to obliterate the need to apply $(I - 1/2)$ modulation frequencies for samples with spin I, we have recently introduced a frequency swept FAM train ('SW-FAM'), where the durations of the RF pulse pairs are changed within the pulse train [22]. The SW-FAM train has been shown to give good signal enhancement for the MAS, and particularly the static, spectra of ^{23}Na ($I = 3/2$), ^{23}Al ($I = 5/2$), ^{45}Sc ($I = 7/2$) [22], and ^{47,49}Ti ($I = 5/2, 7/2$) [23]. The purpose of this paper is to explore the application of FAM-type trains for spin population transfer in static samples in more detail. The RF distributions generated by different varieties of FAM pulse trains are compared, and it is shown that a better signal-enhancement performance can be obtained by sweeping the modulation frequencies linearly over the pulse pairs, instead of adding constant time increments as in the original SW-FAM scheme.

2. Experimental

All ^{27}Al spectra discussed in this work have been acquired on a VARIAN INOVA 400 spectrometer, with a Larmor frequency of $\nu_0(^{27}\mathrm{Al}) = 104.167$ MHz, using a CHEMAGNETICS 4 mm MAS probe. The samples were packed inside the MAS rotor, but not spun. For spectra acquisition, a Hahn-echo sequence with an echo delay of 125 μs and a 16-step phase cycle was used, preceded by the respective FAM trains for spin population transfer, with the central-transition RF nutation frequencies being $\nu_{\mathrm{nut}}(\mathrm{FAM}) = 76$ kHz, and $\nu_{\mathrm{nut}}(\mathrm{echo}) = 42$ kHz. To avoid detection of unwanted coherences, the pulses of the SW-FAM trains were phase-cycled in conformity with the phase of the π/2 pulse of the echo sequence (i.e., $0° + \Phi_{\pi/2}$ and $180° + \Phi_{\pi/2}$). A recycle delay of 15 s was used to avoid saturation effects, and the number of acquired transients was 64 for all spectra.

3. Results and discussion

3.1. Frequency distributions of FAM pulse trains

The resonance frequency of a quadrupolar nucleus with spin I depends on the orientation of the principal axis system of the electric field gradient tensor relative to the external magnetic field. In a polycrystalline (powder) sample, the resonance frequencies of the individual crystallites are statistically oriented over all orientations, and superimpose to produce a characteristic "powder pattern" lineshape.

A FAM pulse train consisting of uniform pulse and interpulse durations (also designated as "FAM-I"), produces only one modulation frequency ($1/\tau$), as shown in Fig. 2B. In a static sample, a FAM-I train can therefore affect the satellite transitions only for a subset of crystallites with suitable orientations. SW-FAM trains, on the other hand, have varying pulse durations (see Fig. 2A) and hence

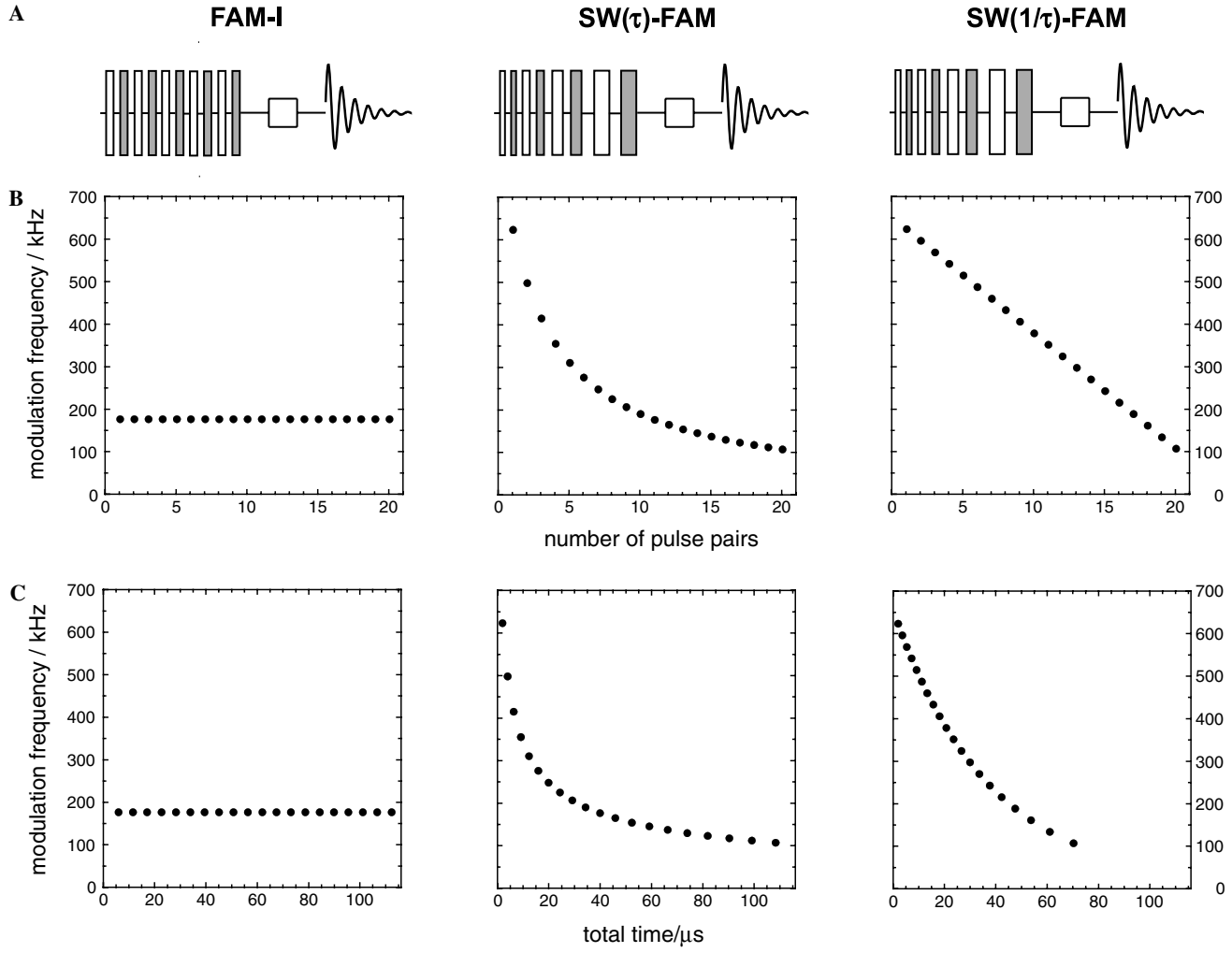

Fig. 2. Modulation frequencies generated by fast amplitude-modulated RF pulse trains with 20 pulse pairs. (Left) FAM-I train with constant modulation period of $4\tau_p = 5.6$ μs; (Centre) SW(τ)-FAM train with constant time increment; (Right) SW($1/\tau$)-FAM pulse train with constant frequency increment. Both SW-FAM trains sweep a modulation range from $\tau_p^0 = 0.4$ to $\tau_p^{19} = 2.3$ μs, corresponding to a sweep width of 516 kHz. A schematic representation of the RF pulse progression is displayed in part (A), together with a read pulse and the resulting FID (alternating white and grey colours signify the 180° phase shift). The modulation frequencies of the RF trains are plotted as: (B) a function of pulse pair progression; (C) a function of the total train duration (in μs).

generate a distribution of modulation frequencies, which can influence a larger range of crystallite orientations. In the original SW-FAM scheme [22], constant time increments Δ are added to the duration of both the RF pulses τ_p and interpulse delays, the delays being chosen to be equal to τ_p for simplicity. Thus, a pulse train starting with a modulation period of $\tau^0 = 4\tau_p^0$ for the first FAM pulse pair, would finish with a modulation period $\tau^{N-1} = 4\tau_p^{N-1}$ after the execution of N pulse pairs, with $\tau_p^{N-1} = \tau_p^0 + (N-1)\Delta$. (For the sake of conceptual clarity, we slightly deviate from previously used conventions [22,23] and designate with N the total number of pulse *pairs*, and enumerate the successive pulse pairs starting from zero, $n = 0, 1, 2, \ldots, N-1$.) During the sweep, such a pulse train produces a curved distribution of frequencies $(1/\tau^n)$, as a result of the modulation periods τ being incremented linearly, as shown in Fig. 2B. We will therefore refer to such pulse trains as SW(τ)-FAM, some characteristics of which are summarised in Table 1.

An alternative approach is to generate a frequency distribution which is linear with respect to the pulse pair progression. This can be achieved by incrementing the modulation frequencies such that for the nth pulse pair, $(1/\tau^n) = a'(n+1) + b'$. The resulting pulse train (see Fig. 2B) will be designated as SW($1/\tau$)-FAM. The required durations of the RF pulses τ_p^n within a SW($1/\tau$)-FAM train depend on the desired sweep width and the overall number of pulse pairs. The necessary calculations (see Table 1) can be readily performed by the pulse program of the spectrometer, although the demand for rapid execution of consecutive pulse pairs may require pre-calculation and storage of the τ_p^n's [24]. As a result of the changed distribution of modulation frequencies, a SW($1/\tau$)-FAM train completes a given sweep window faster than the original SW(τ)-FAM sequence, as shown in Fig. 2C.

In the absence of sample rotation, the spin population transfer process is driven solely by the RF modulation. Thus, for static spectra, some insight into the working mechanism of FAM sequences can be gained by inspecting the frequency distributions generated by the pulse trains. To this end, the Fourier transforms of the time-domain representation of the respective FAM train have been calculated (see Appendix A for details). The resulting complex frequency-domain functions $\mathcal{F}(\omega)$ for typical FAM-I, SW(τ)-FAM and SW($1/\tau$)-FAM trains are depicted in Fig. 3. The real (Fig. 3A) and imaginary (Fig. 3B) parts of the $\mathcal{F}(\omega)$'s can be thought of as the x and y components of the RF, respectively. The best way to assess the width of the frequency distribution and the intensity of the RF is to plot the absolute value of the frequency representation $\sqrt{\mathcal{F}_{\text{real}}^2 + \mathcal{F}_{\text{imag}}^2}$, as shown in Fig. 3C.

A FAM-I train with constant pulse (and interpulse) durations τ_p modulates the carrier frequency ω_0 with a single frequency $\omega = 2\pi/(4\tau_p)$, which generates sidebands at $+\omega$ and $-\omega$ (plus weak higher-order sidebands at $\pm 3\omega$). As can be seen from Fig. 3, the sidebands generated by a FAM-I train with $N = 35$ are very narrow, and can thus influence only a small number of crystallites in a static powder sample. This is reflected in the poor signal enhancement performance of FAM-I pulse trains for static spectra, even when using two FAM-I blocks with different modulation frequencies for spin-5/2 nuclei, as reported earlier [22]. In contrast, the frequencies generated by SW(τ)-FAM and SW($1/\tau$)-FAM pulse trains are spread over the range determined by their sweep width, i.e., by the choice of the first and last pulse durations. It can be seen from Fig. 3C that the frequency distribution of a SW($1/\tau$)-FAM train is considerably flatter than that of a SW(τ)-FAM train, because in the latter a larger proportion of pulse pairs contributes to the lower frequencies of the sweep. The improved distribution of RF intensity should lead to better and more robust signal-enhancement performance for SW($1/\tau$)-FAM pulse trains. It should be kept in mind, however, that spin response in NMR is in general a non-linear phenomenon. Therefore, the distributions shown in Fig. 3 should be considered only as an approximation to gauge the effect of the pulse sequences on the spin system.

3.2. Comparison of signal enhancement: experimental

To compare the signal-enhancement performance of the SW($1/\tau$)-FAM to that of the original SW(τ)-FAM scheme experimentally, static ^{27}Al NMR spectra of corundum (α-Al_2O_3), aluminium acetylacetonate ($Al(CH_3COCHCOCH_3)_3$), and barium aluminate ($BaAl_2O_4$) were recorded. The intensity of the ^{27}Al central-transition signal acquired with a simple Hahn echo was normalised to unity, and compared to the signal intensity obtained by preceding the Hahn-echo acquisition with SW-FAM trains consisting

Table 1
Properties of SW-FAM pulse trains with N pulse pairs, and equal duration of RF pulse and interpulse delays

	SW(τ)-FAM	SW($1/\tau$)-FAM
Sweep width	$(\tau_p^{N-1} - \tau_p^0)/(4\tau_p^{N-1}\tau_p^0)$	
Specified parameters	$\tau_p^0, \tau_p^{N-1}, N$	
Derived parameters	$\Delta = (\tau_p^{N-1} - \tau_p^0)/(N-1)$	$a = (\tau_p^0 - \tau_p^{N-1})/(\tau_p^{N-1}\tau_p^0(N-1))$ $b = (1/\tau_p^0) - a$
Duration of nth pulse ($n = 0, 1, 2, \ldots, N-1$)	$\tau_p^n = \tau_p^0 + n\Delta$	$\tau_p^n = 1/[a(n+1) + b]$
Total duration of train	$4N\tau_p^0 + 2\Delta(N-1)N$	$\sum_{n=0}^{N-1} 4/[a(n+1) + b]$

τ_p^0, duration of first pulse; τ_p^{N-1}, duration of last pulse.

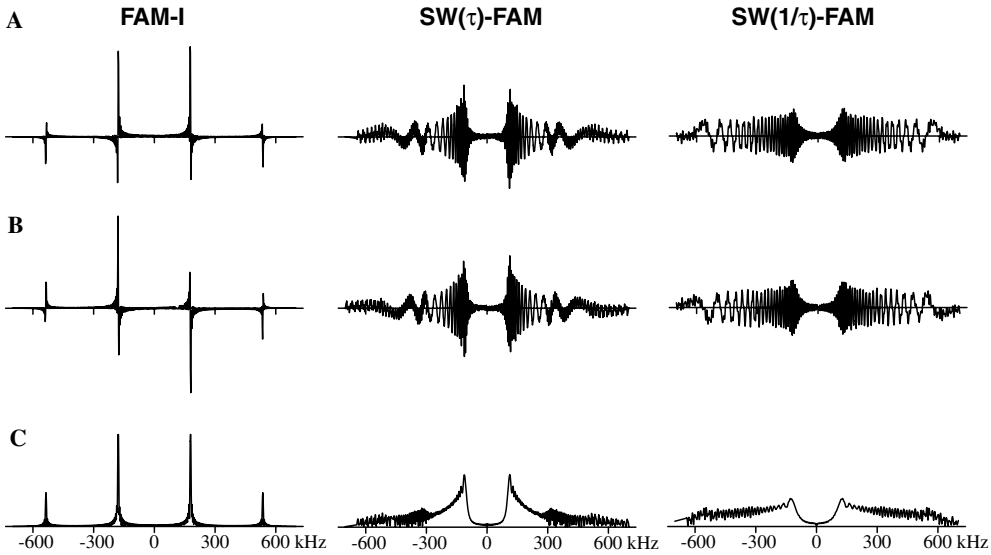

Fig. 3. Frequency distributions generated by FAM-I ($\tau_p = 1.4$ μs), SW(τ)-FAM and SW($1/\tau$)-FAM pulse trains ($\tau_p^0 = 0.4$ μs, $\tau_p^{34} = 2.5$ μs, i.e., sweep width = 525 kHz), with $N = 35$ pulse pairs. For a clearer view, the intensity (in arbitrary units) of the SW-FAM representations is doubled with respect to the FAM-I plots. (A) Real part of the complex frequency-domain functions $\mathcal{F}(\omega)$ generated by the respective RF trains. (B) Imaginary part of the $\mathcal{F}(\omega)$'s. (C) Absolute-mode representation of the $\mathcal{F}(\omega)$'s.

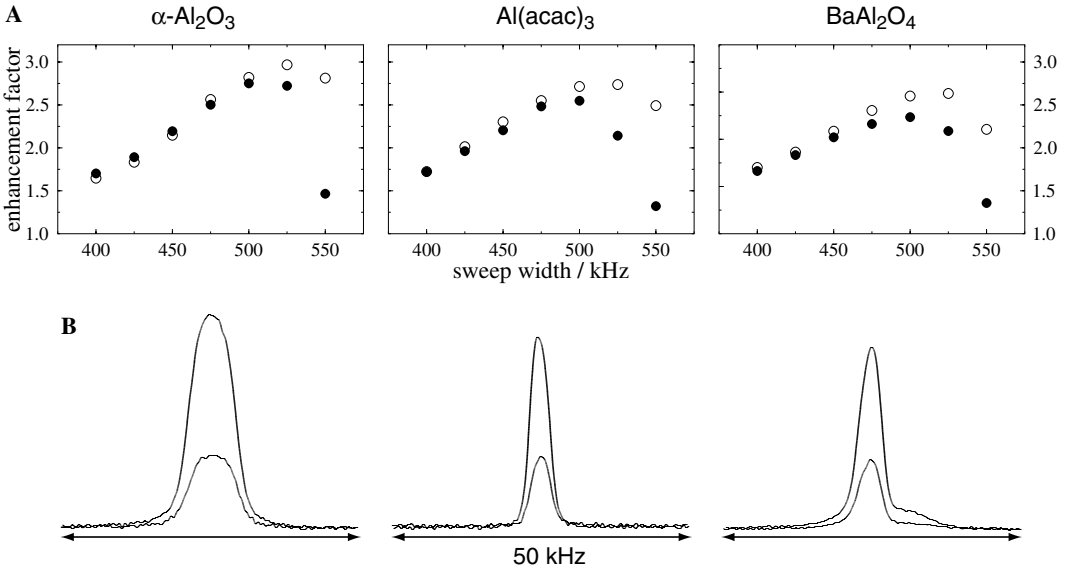

Fig. 4. Central-transition signal enhancement of static ^{27}Al NMR spectra of corundum (left), aluminium acetylactonate (centre), and barium aluminate (right) by spin population transfer from the satellite transitions. (A) Enhancement factors normalised to the signal intensity of the Hahn-echo spectrum for SW($1/\tau$)-FAM (open circles) and SW(τ)-FAM (closed circles) pulse trains with 35 pulse pairs and $\tau_p^0 = 0.4$ μs, as a function of the modulation frequency sweep width. Because of the time resolution of the pulse programmer, the sweep widths are approximate. For the used sweep widths (ca. 400, 425, 450, 475, 500, 525, and 550 kHz), the actual durations of the last pulses were $\tau_p^{34} = 1.1125$, 1.250, 1.425, 1.6625, 2.0, 2.5, and 3.3375 μs. (B) Static ^{27}Al NMR with the best enhancement (as compared to the also shown Hahn-echo spectra), obtained with a SW($1/\tau$)-FAM pulse train ($N = 35$, $\tau_p^0 = 0.4$ μs, $\tau_p^{34} = 2.5$ μs, i.e., sweep width = 525 kHz).

of $N = 35$ pulse pairs, using an array of increasing sweep widths from 400 to 550 kHz. In Fig. 4A, it can be seen that the SW($1/\tau$)-FAM sequence delivers better enhancement factors than SW(τ)-FAM for all three compounds investigated, and also shows a more robust performance with respect to the employed sweep width. The best signal enhancements achievable with our experimental set-up are summarised in Table 2 for both SW($1/\tau$)-FAM (corresponding spectra also shown in Fig. 4B) and SW(τ)-FAM. To evaluate these results, the theoretical limits of signal enhancement by spin population transfer for spin I should be recalled: complete saturation of the satellite transitions leads to an enhancement of $I + 1/2$, whereas perfect inversion gives a factor of $2I$. By applying a SW($1/\tau$)-FAM train before the acquisition of ^{27}Al spectra ($I = 5/2$), the limit of complete saturation $I + 1/2 = 3$ is practically reached for

Table 2
Best enhancement of the central-transition signal of static ^{27}Al NMR spectra obtained by preceding Hahn-echo acquisition by SW-FAM modulated pulse trains

Sample	χ (MHz)	η	Reference	Best FAM enhancement	
				SW(τ)	SW($1/\tau$)
α-Al_2O_3	2.403	0.000	[26]	2.75	2.97
$Al(CH_3COCHCOCH_3)_3$	3.03	0.15	[27]	2.55	2.74
$BaAl_2O_4$	2.4	0.4	[28]	2.36	2.63

The ^{27}Al quadrupolar coupling constants χ and asymmetry parameters η were taken from the listed references. The best enhancement (last column) relative to the signal intensity of the Hahn-echo spectrum was obtained for sweep widths of 500 kHz for SW(τ)-FAM and 525 kHz for SW($1/\tau$)-FAM (see Fig. 4A).

corundum, and is approached for the other compounds (see Table 2). However, reaching this limit does necessarily imply that the satellite transitions of all crystallites in the sample have indeed been saturated. Kentgens et al. [13] have analysed the combined effect of DFS and MAS on powder samples in detail, and concluded that different degrees of saturation and inversion are distributed randomly over all orientations of the sphere. While there is no sample rotation in our experiments, a time dependence is introduced by the sweep of the modulation frequency of the SW-FAM pulse trains. Therefore, the observed enhancement is most likely a result of partial saturation and inversion, dispersed among the affected crystallites.

As for the performance of other spin population transfer techniques, Wasylishen et al. [15] have reported complete inversion of the satellite transitions with a corresponding signal enhancement of $2I$ (with $I = 3/2$) for static ^{23}Na spectra of single crystals. This remarkable efficiency is however expected to deteriorate for polycrystalline samples. A more relevant comparison in the current context is a result described by Schurko et al. [25] for static spectra of ^{85}Rb (with $I = 5/2$, in contrast to the more frequently measured isotope ^{87}Rb with $I = 3/2$). Preceding a Hahn-echo acquisition by DFS, a signal enhancement factor of 2.9 was obtained [25], which is similar to the findings presented here. It may be noted that, while the duration of the SW($1/\tau$)-FAM train giving the best signal enhancement was just 125 μs, the hyperbolic secant pulse employed in [15] lasted for 600 μs, and the DFS used in [25] took 1200 μs to complete. Such long execution times place higher demands on probe stability, and may also lead to problems in spin systems with short relaxation times.

3.3. Comparison of signal enhancement: simulations

To systematically investigate the signal-enhancement performance of FAM sequences for a range of quadrupolar coupling constants $\chi = (e^2qQ)/h$ and asymmetry parameters η, numerical simulations over a grid with $\chi = 0, \ldots, 4$ MHz (step 0.5 MHz) and $\eta = 0, \ldots, 1$ (step 0.25) were carried out using the SIMPSON package [29]. The static ^{27}Al central-transition signal was calculated considering 28656 powder orientations according to the ZCW scheme [30–32], over a spectral width of 32 kHz, with the Larmor frequency identical to the experimental work. The central-transition RF nutation frequencies used for preceding FAM train and single read pulse were $\nu_{\mathrm{nut}}(\mathrm{FAM}) = 60$ kHz, and $\nu_{\mathrm{nut}}(\mathrm{read}) = 30$ kHz, respectively. To obtain enhancement factors, the total signal intensity of the spectrum with FAM train and read pulse was compared to the corresponding single-pulse spectrum, by summing up the intensities of all calculated spectral points, $\sum_i I(\nu_i)$, with $i = 1, \ldots, 2048$.

Performance of the FAM pulse trains was optimised for the midpoint of the investigated grid, i.e., for $\chi = 2.0$ MHz and $\eta = 0.5$. Besides the obvious criterion of enhanced intensity, the reproduction of the correct line shape is also important. SW-FAM pulse trains can be optimised by varying 4 parameters: starting value of the modulation frequency (τ_p^0), width of frequency sweep (τ_p^{N-1}), rate of sweep (number of pulse pairs N), and RF field strength. These parameters also determine the adiabaticity of the SW-FAM sequence: the RF sweep is said to traverse a transition "adiabatically" when changes in the frequency are slow enough for the spin system to follow the effective field [33]. The adiabaticity of RF sweeps for multi-level systems such as quadrupolar nuclei with half-integer spin is a complex problem [13], a detailed discussion being outside the scope of this paper. While the numerical simulation of the single-pulse spectrum produced nearly ideal lineshapes, some deviations from these lineshapes were observed in the FAM-enhanced spectra, depending on the FAM pulse train parameters. One possible reason for these deviations could be a breach of the adiabaticity conditions, as the duration of SW-FAM trains is generally quite short. In the context of the current work, it is helpful to quantify the lineshape differences produced by the numerical calculations. Thus, the intensities of both the FAM-enhanced (I_{FAM}) and the single-pulse spectrum (I_{SP}) were normalised to a common factor C, such that $I^C(\nu_i) = [C/\sum_i I(\nu_i)] \cdot I(\nu_i)$, for every intensity point in the spectrum. Then, a root-mean-square variation between the spectra was computed as $\mathrm{r.m.s.} = \sqrt{\sum_i (I^C_{\mathrm{FAM}}(\nu_i) - I^C_{\mathrm{SP}}(\nu_i))^2}$, and C being chosen such as to produce convenient numbers for the r.m.s. values of all investigated spectra. For the SW-FAM trains, a good compromise between enhancement and lineshape quality was found using parameters close to those used in the experiments. Similarly, a good set of parameters was found for the FAM-I pulse train with two modulation blocks, starting from the experimental values listed in [22]. The resulting spectra are shown in Fig. 5 with the pulse train parameters listed in the figure caption.

The performance of the thus obtained pulse trains was subsequently tested over the entire $\{\chi, \eta\}$ grid, without further optimisation. The results of these numerical simulations are summarised in Fig. 6. As expected, the spin population transfer induced by a FAM-I train (even with two modulation frequencies) is not very efficient, with the

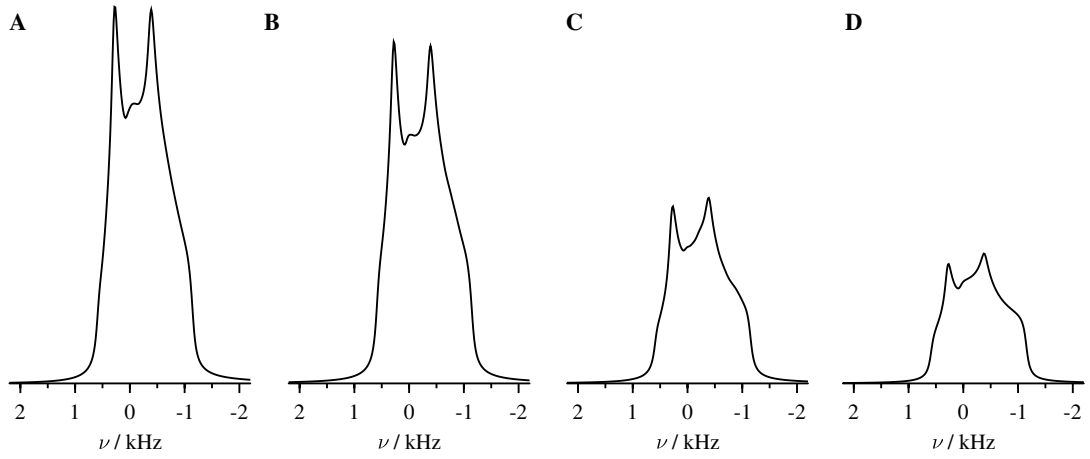

Fig. 5. Numerical simulation of central-transition signal enhancement of static ^{27}Al NMR spectra by FAM sequences: performance optimisation for $\chi = 2.0$ MHz and $\eta = 0.5$. (A) SW$(1/\tau)$-FAM pulse train with $N = 50$, $\tau_p^0 = 0.4$ μs, $\tau_p^{49} = 2.5$ μs (sweep width 525 kHz). The obtained enhancement factor is 2.64, and the r.m.s. variation from single-pulse spectrum is 0.94 (see text for details). (B) SW(τ)-FAM pulse train with $N = 50$, $\tau_p^0 = 0.4$ μs, $\tau_p^{49} = 2.5$ μs (sweep width 525 kHz). The obtained enhancement factor is 2.46, and the r.m.s. variation from single-pulse spectrum is 0.80. (C) FAM-I pulse train with two modulation blocks, $\tau_p(1) = 1.0$ μs, $\tau_p(2) = 1.6$ μs, with $N = 25$ each. The obtained enhancement factor is 1.37, and the r.m.s. variation from single-pulse spectrum is 0.45. (D) Single-pulse spectrum.

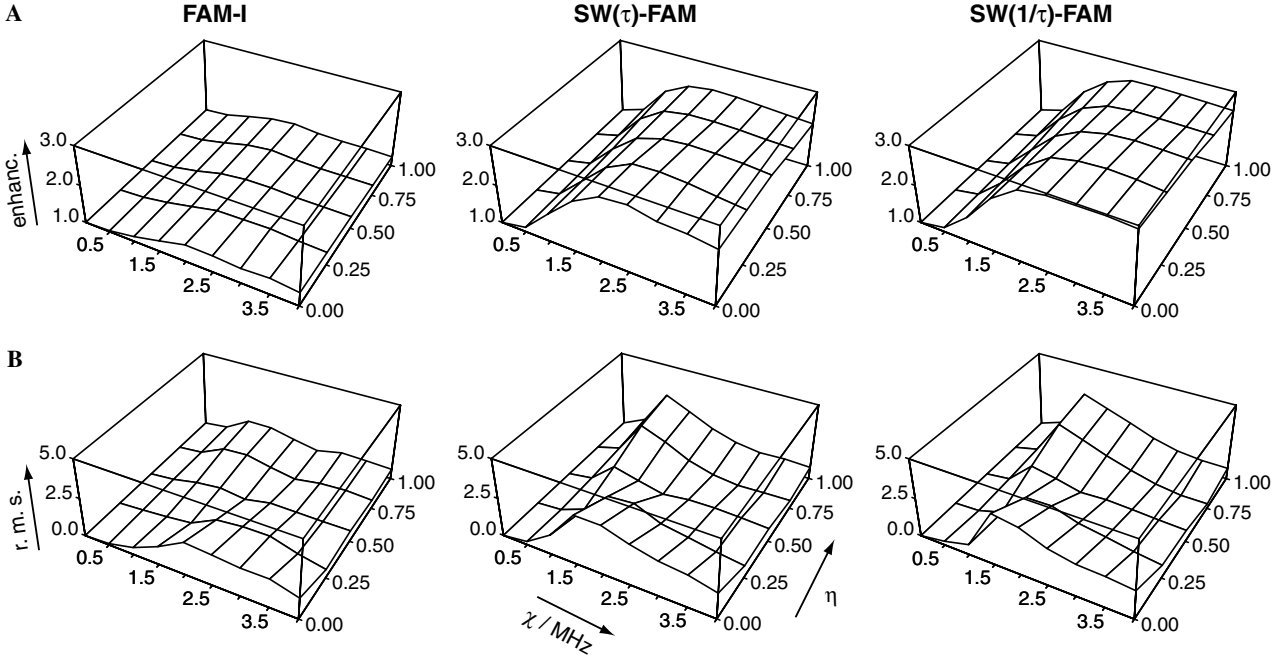

Fig. 6. Numerical simulation of central-transition signal enhancement of static ^{27}Al NMR spectra by FAM sequences: performance over a grid of $\chi = 0, \ldots, 4$ MHz (step 0.5 MHz) and $\eta = 0, \ldots, 1$ (step 0.25). The pulse train parameters used for FAM-I (left), SW(τ)-FAM (centre) and SW$(1/\tau)$-FAM (right) are those specified in Fig. 5. (A) Enhancement factors relative to the intensity of the single-pulse spectrum. (B) r.m.s. variation from single-pulse spectrum (see text for details).

enhancement factor not exceeding 1.5 anywhere on the grid. Since the spectra are not much affected by FAM-I, the r.m.s. variation of the lineshape is comparatively small. In contrast, both SW-FAM sequences deliver enhancement factors close to the saturation value of $I + 1/2 = 3$, in good agreement with the experimental results discussed above. When averaging over the entire grid (see Table 3), the SW$(1/\tau)$ train somewhat outperforms the SW(τ) sequence, again in accordance with the experimental results shown in Fig. 4. The average r.m.s. lineshape variation is practically identical for both SW-FAM sequences, and overall larger than the one observed for the FAM-I train. As one would expect, the r.m.s. surfaces in Fig. 6B all show a small inflection at the midpoint, i.e., the $\{\chi,\eta\}$ combination for which the respective FAM sequences have been optimised. Similarly, any r.m.s. variation on the grid can be diminished by further optimising the pulse trains for the $\{\chi,\eta\}$ combination in question. Also, it should be noted that, FAM-enhanced static spectra of 4 different nuclei (^{23}Na, ^{27}Al, ^{45}Sc, and ^{49}Ti) and eight compounds have been reported so far

Table 3
Numerical simulation of central-transition signal enhancement of static ^{27}Al NMR spectra by FAM sequences: average performance over the grid shown in Fig. 6, calculated for $\chi = 0.5, \ldots, 4$ MHz (no enhancement is expected for $\chi = 0$ MHz) and $\eta = 0, \ldots, 1$

Pulse train	Avg. enhancement	Avg. r.m.s. variation
FAM-I	1.277	0.821
SW(τ)-FAM	2.178	1.341
SW($1/\tau$)-FAM	2.375	1.348

The pulse train parameters were optimised for the midpoint of the grid ($\chi = 2.0$ MHz and $\eta = 0.5$), and are listed in Fig. 5.

(in [22,23] and this work), without any appreciable lineshape distortions, indicating that the lineshape problem is less prevalent in experiments. However, the deviations of lineshape found by numerical simulations may also manifest themselves in experiments. Recently, distortions of static ^{23}Na lineshapes by SW(τ)-FAM have indeed been reported by Jerschow and co-workers [4]. It remains to be investigated whether the application of the improved SW($1/\tau$)-FAM sequence or a fortunate choice of the pulse train parameters can alleviate these lineshape problems, or whether they are a result of the same problems underlying the deviations observed in our simulations. In any event, further investigation of the detailed mechanisms of spin population transfer mediated by FAM-type pulse trains seems to be worthwhile, and is currently in progress.

4. Conclusions

Fast amplitude-modulated RF pulse trains with swept modulation frequency (SW-FAM) can be utilised for enhancing the central-transition signal of half-integer spin nuclei in static spectra by population transfer. In this work, we have demonstrated that for static spectra, the performance of the original SW(τ)-FAM sequence with constant time increments [22,23] can be improved by distributing the modulation frequency linearly over the pulse pairs, which is done in the SW($1/\tau$)-FAM sequence. Comparison of Fourier transforms shows that the RF intensities of SW($1/\tau$)-FAM trains are more evenly spread over the sweep window than those of SW(τ)-FAM trains. For static spectra, no rotor-induced modulations exist, and the population transfer is mediated by RF pulses only. The superior RF intensity distribution of SW($1/\tau$)-FAM trains translates into better population transfer efficiency, and signal enhancement factors up to the limit of complete saturation ($I + 1/2$) were obtained both by experiment and numerical simulations for static NMR spectra of ^{27}Al ($I = 5/2$). It may be noted that the improved performance of SW($1/\tau$)-FAM does not necessarily extend to MAS spectra: here, the original SW(τ)-FAM sequence may still give better results. The reasons for this are currently under investigation and will be described in a future publication.

The central-transition signal of static spectra can also be enhanced by double-frequency sweeps (DFS) [9–13] and hyperbolic secant pulses [15]. Whereas SW-FAM and DFS work along similar physical principles, the methods of generating the desired frequency profile are different. SW-FAM is using a series of hard RF pulses, which are easily produced by the pulse programmer of a standard solid-state NMR spectrometer, without the need for special hardware or pulse shaping. At the same time, the use of hard RF pulses limits the sweep ranges accessible to SW-FAM trains, which may compromise the achievable enhancement factors and/or lead to lineshape problems. However, because of the relative ease of use and implementation, the authors believe SW-FAM trains to be a viable alternative to other methods.

Note added in proof

While this paper was being reviewed, the first applications of hyperbolic secant (HS) pulses to static powder samples with $I = 5/2$ were reported by Wasylishen et al. [34]. For ^{27}Al spectra of aluminium acetylacetonate, a signal enhancement factor of 4.0 was attained, corresponding to a mix of saturation and inversion of the satellite transitions. Complete inversion (with a corresponding signal enhancement of $2I$) hence remains an elusive goal for powder samples. Similar to the enhanced static spectra discussed in this work, the HS-enhanced spectra display some small lineshape distortions [34].

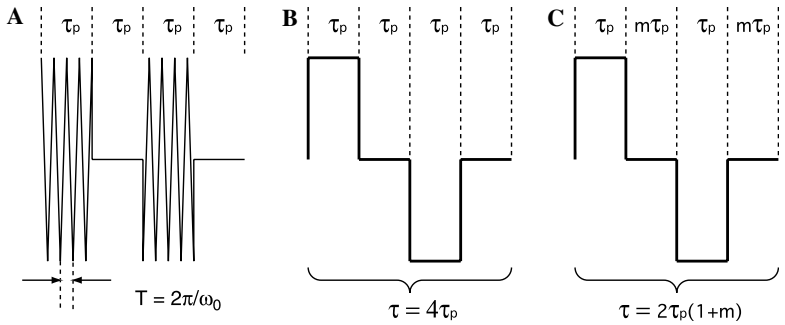

Fig. 7. Representations of a FAM-I pulse pair: (A) Two RF pulses with Larmor frequency ω_0, and a 180° phase shift. The duration τ_p of RF pulses and interpulse delays is equal. (B) Rectangular representation of the pulse pair shown in (A), with ω_0 set to zero. (C) Rectangular representation of a FAM-I pulse pair, with pulse duration τ_p, and the interpulse delay being an arbitrary multiple or fraction $m\tau_p$ of it.

Acknowledgments

P.K.M. acknowledges assistance from the Department of Science and Technology, India, under SERC FAST Track Scheme.

Appendix A

A.1. Fourier transformation of FAM-I pulse trains

The simplest FAM pulse train ("FAM-I") is formed by a pair of radio-frequency (RF) pulses with Larmor frequency ω_0 and duration τ_p, separated by interpulse delays of equal duration (see Fig. 7A). Between consecutive RF pulses, a phase shift is applied to ω_0, so that the pulse pair consists of a x pulse with 0° phase, and a $-x$ pulse with 180° phase. The time domain function $f'(t)$ of such a pulse pair can be described by:

$$f'(t) = \begin{cases} \cos\omega_0 t, & 0 \leqslant t \leqslant \tau_p, \\ -\cos\omega_0 t, & 2\tau_p \leqslant t \leqslant 3\tau_p, \\ 0, & \text{otherwise.} \end{cases}$$

As our main interest is the modulation generated by the 180° phase shift, it is convenient to represent a FAM train by simple rectangular shapes, as shown in Fig. 7B. One way of formally producing this representation is to set ω_0 to zero, so that

$$f(t) = \begin{cases} 1, & 0 \leqslant t \leqslant \tau_p, \\ -1, & 2\tau_p \leqslant t \leqslant 3\tau_p, \\ 0, & \text{otherwise.} \end{cases}$$

As a result of this simplification, the Fourier transformed function of $f(t)$ will be centered around zero, and not around the Larmor frequency ω_0, which (with reversed signs) corresponds to the way NMR spectra are usually displayed.

In principle, the desired modulation can be created without the interpulse ('window') delays between the consecutive RF pulses of a FAM-I train. These window delays are however needed to allow the NMR hardware sufficient time for shifting the phase before generating the next RF pulse. For a more general treatment, we are going to use a rectangular representation of a FAM-I pulse pair, where the duration of the interpulse delay is an arbitrary fraction $m\tau_p$ of the pulse duration τ_p, as shown in Fig. 7C. For $m = 1$, we have the familiar situation of equal pulse and window duration; for $m = 0$, the FAM-I train is 'windowless.' The time domain function $f(t)$ of one such pulse pair is:

$$f(t) = \begin{cases} 1, & 0 \leqslant t \leqslant \tau_p, \\ -1, & \tau_p(1+m) \leqslant t \leqslant \tau_p(2+m), \\ 0, & \text{otherwise.} \end{cases}$$

The frequency representation of $f(t)$ is given by its Fourier transform, $\mathcal{F}(\omega)$ (for one pulse pair):

$$\begin{aligned} \mathcal{F}(\omega) &= \int f(t)\mathrm{e}^{-\mathrm{i}\omega t}\mathrm{d}t = \int_0^{\tau_p} \mathrm{e}^{-\mathrm{i}\omega t}\mathrm{d}t - \int_{\tau_p(1+m)}^{\tau_p(2+m)} \mathrm{e}^{-\mathrm{i}\omega t}\mathrm{d}t \\ &= \frac{1}{\mathrm{i}\omega}\left[1 - \mathrm{e}^{-\mathrm{i}\omega\tau_p} - \mathrm{e}^{-\mathrm{i}(1+m)\omega\tau_p} + \mathrm{e}^{-\mathrm{i}(2+m)\omega\tau_p}\right]. \end{aligned} \tag{1}$$

For a FAM train consisting of N identical pulse pairs, $\mathcal{F}(\omega)$ is given by

$$\begin{aligned} \mathcal{F}(\omega) &= \frac{1}{\mathrm{i}\omega}\sum_{n=0}^{N-1} \mathrm{e}^{-\mathrm{i}2n(1+m)\omega\tau_p} \\ &\quad \times \left[1 - \mathrm{e}^{-\mathrm{i}\omega\tau_p} - \mathrm{e}^{-\mathrm{i}(1+m)\omega\tau_p} + \mathrm{e}^{-\mathrm{i}(2+m)\omega\tau_p}\right] \\ &= \frac{1}{\mathrm{i}\omega}\left[1 - \mathrm{e}^{-\mathrm{i}\omega\tau_p} - \mathrm{e}^{-\mathrm{i}(1+m)\omega\tau_p} + \mathrm{e}^{-\mathrm{i}(2+m)\omega\tau_p}\right] \\ &\quad \times \sum_{n=0}^{N-1} \left(\mathrm{e}^{-\mathrm{i}2(1+m)\omega\tau_p}\right)^n. \end{aligned} \tag{2}$$

The sum of exponentials in the above equation can be substituted according to

$$\sum_{n=0}^{N-1} \left(\mathrm{e}^{-\mathrm{i}2(1+m)\omega\tau_p}\right)^n = \frac{1 - \mathrm{e}^{-\mathrm{i}2N(1+m)\omega\tau_p}}{1 - \mathrm{e}^{-\mathrm{i}2(1+m)\omega\tau_p}} \tag{3}$$

which leads to a general expression for the frequency function $\mathcal{F}(\omega)$ of a FAM-I train with N pulse pairs, pulse durations τ_p, and interpulse delays $m\tau_p$

$$\mathcal{F}(\omega) = \frac{1}{\mathrm{i}\omega}\frac{\left(1 - \mathrm{e}^{-\mathrm{i}\omega\tau_p}\right)\left(1 - \mathrm{e}^{-\mathrm{i}2N(m+1)\omega\tau_p}\right)}{1 + \mathrm{e}^{-\mathrm{i}(m+1)\omega\tau_p}} \tag{4}$$

A.2. Fourier transformation of SW-FAM pulse trains

For SW-FAM pulse trains, a frequency sweep effect is introduced by constantly varying the duration of the RF pulse pairs [22]. As the modulation frequency generated by a FAM train depends only on the overall modulation period, the pulse sequences are usually implemented with equal duration for the RF pulses and interpulse delays. This simplifying strategy will also be used for the following derivation of Fourier transforms for SW-FAM pulse trains.

For a SW(τ)-FAM train, a constant time increment Δ is added to the duration of both RF pulses and interpulse delays, when progressing from one pulse pair to the next. For the first pulse pair, the Fourier transform is still given by Eq. (1) (with $m = 1$). For the next pulse pairs, however, the integration boundaries begin to shift because of the added time increments Δ. This shift can be described for each of the boundaries in terms of the summation variable n

$$\begin{aligned} &\text{start of } x \text{ pulse}, && 2n(n-1)\Delta, \\ &\text{end of } x \text{ pulse}, && n(2n-1)\Delta, \\ &\text{start of } -x \text{ pulse}, && 2n^2\Delta, \\ &\text{end of } -x \text{ pulse}, && n(2n+1)\Delta. \end{aligned}$$

Consequently, the Fourier transform $\mathcal{F}^\tau(\omega)$ of a SW(τ)-FAM train with N pulse pairs is given by

$$\mathcal{F}^{\tau}(\omega) = \frac{\mathrm{i}}{\omega}\sum_{n=0}^{N-1}\left[\mathrm{e}^{-\mathrm{i}\omega\left[4n\tau_p+2n(n-1)\Delta\right]} - \mathrm{e}^{-\mathrm{i}\omega\left[(4n+1)\tau_p+n(2n-1)\Delta\right]} - \mathrm{e}^{-\mathrm{i}\omega\left[(4n+2)\tau_p+2n^2\Delta\right]} + \mathrm{e}^{-\mathrm{i}\omega\left[(4n+3)\tau_p+n(2n+1)\Delta\right]}\right]. \quad (5)$$

Since the summation variable n occurs in non-linear expressions in the exponentials, we cannot utilise a relation similar to Eq. (3) to further simplify the above equation.

For a SW$(1/\tau)$-FAM train, a linear sweep in frequency is produced by calculating the duration of pulses and interpulse delays for each pulse pair according to $(1/\tau_p^n) = a(n+1)+b$. The parameters a and b depend on the desired characteristics of the frequency sweep (see Table 1). For the first pulse pair, the Fourier transform is again given by Eq. (1), with $m = 1$ and $\tau_p = 1/(a+b)$. For the $(n+1)$th pulse pair of a SW$(1/\tau)$-FAM train, the sum of the duration of all previous pulse pairs is given by

$$s_k = \sum_{k=1}^{n}\frac{4}{ak+b}. \quad (6)$$

The Fourier transform $\mathcal{F}^{1/\tau}(\omega)$ of a SW$(1/\tau)$-FAM train with N pulse pairs can hence be described by

$$\mathcal{F}^{1/\tau}(\omega) = \frac{\mathrm{i}}{\omega}\sum_{n=0}^{N-1}\left\{\mathrm{e}^{-\mathrm{i}\omega s_k} - \mathrm{e}^{-\mathrm{i}\omega\left[s_k+\frac{1}{(n+1)a+b}\right]} - \mathrm{e}^{-\mathrm{i}\omega\left[s_k+\frac{2}{(n+1)a+b}\right]} + \mathrm{e}^{-\mathrm{i}\omega\left[s_k+\frac{3}{(n+1)a+b}\right]}\right\}. \quad (7)$$

Thus, the frequency distribution of SW-FAM trains with a given sweep width $[1/(4\tau_p^0) - 1/(4\tau_p^{N-1})]$ and any number of pulse pairs N can be calculated from Eq. (5) for SW(τ)-FAM trains with linear time increment, and from Eq. (7) for SW$(1/\tau)$-FAM trains with linear frequency increment. The involved summations are readily carried out with the aid of a computer [24].

References

[1] K.J.D. MacKenzie, M.E. Smith, Multinuclear Solid-State NMR of Inorganic Materials, Pergamon Press, Oxford, 2002.

[2] E.R. Andrew, Magic angle spinning in solid state n.m.r. spectroscopy, Phil. Trans. R. Soc. A 299 (1981) 505–520.

[3] C. Gervais, D. Veautier, M.E. Smith, F. Babonneau, P. Belleville, C. Sanchez, Solid state ^{47,49}Ti, ^{87}Sr and ^{137}Ba NMR characterisation of mixed barium/strontium titanate perovskites, Solid State Nucl. Magn. Reson. 26 (2004) 147–152.

[4] R. Kumar, W. Ling, W. Schoefberger, A. Jerschow, Separated quadrupolar field experiment, J. Magn. Reson. 172 (2005) 209–213.

[5] S. Vega, Y. Naor, Triple quantum NMR on spin systems with $I = 3/2$ in solids, J. Chem. Phys. 75 (1981) 75–86.

[6] J. Haase, M.S. Conradi, Sensitivity enhancement for NMR of the central transition of quadrupolar nuclei, Chem. Phys. Lett. 209 (1993) 287–291.

[7] J. Haase, M.S. Conradi, C.P. Grey, A.J. Vega, Population transfers for NMR of quadrupolar spins in solids, J. Magn. Reson. A 109 (1994) 90–97.

[8] J. Haase, M.S. Conradi, E. Oldfield, Single- and double-resonance experiments of quadrupolar nuclei in solids using sensitivity enhancement of the central transition, J. Magn. Reson. A 109 (1994) 210–215.

[9] E. van Veenendal, B.H. Meier, A.P.M. Kentgens, Frequency stepped adiabatic passage excitation of half-integer quadrupolar spin systems, Mol. Phys. 93 (1998) 195–213.

[10] A.P.M. Kentgens, R. Verhagen, Advantages of double frequency sweeps in static, MAS and MQMAS NMR of spin $I = 3/2$ nuclei, Chem. Phys. Lett. 300 (1999) 435–443.

[11] D. Iuga, H. Schäfer, R. Verhagen, A.P.M. Kentgens, Population and coherence transfer induced by double frequency sweeps in half-integer quadrupolar spin systems, J. Magn. Reson. 147 (2000) 192–209.

[12] H. Schäfer, D. Iuga, R. Verhagen, A.P.M. Kentgens, Population and coherence transfer in half-integer quadrupolar spin systems induced by simultaneous rapid passages of the satellite transitions: a static and spinning single crystal nuclear magnetic resonance study, J. Chem. Phys. 114 (2001) 3073–3091.

[13] D. Iuga, A.P.M. Kentgens, Influencing the satellite transitions of half-integer quadrupolar nuclei for the enhancement of magic angle spinning spectra, J. Magn. Reson. 158 (2002) 65–72.

[14] M.S. Silver, R.I. Joseph, D.I. Hoult, Selective spin inversion in nuclear magnetic resonance and coherent spin optics through an exact solution of the Bloch-Riccati equation, Phys. Rev. A 31 (1985) 2753–2755.

[15] R. Siegel, T.T. Nakashima, R.E. Wasylishen, Signal enhancement of NMR spectra of half-integer quadrupolar nuclei in solids using hyperbolic secant pulses, Chem. Phys. Lett. 388 (2004) 441–445.

[16] P.K. Madhu, A. Goldbourt, L. Frydman, S. Vega, Sensitivity enhancement of the MQMAS NMR experiment by fast amplitude modulation of the pulses, Chem. Phys. Lett. 307 (1999) 41–47.

[17] A. Goldbourt, P.K. Madhu, Multiple-quantum magic-angle spinning: high-resolution solid-state NMR spectroscopy of half-integer quadrupolar nuclei, Monatshefte für Chemie 133 (2002) 1497–1534.

[18] Z. Yao, H.-T. Kwak, D. Sakellariou, L. Emsley, P.J. Grandinetti, Sensitivity enhancement of the central transition NMR signal of quadrupolar nuclei under magic-angle spinning, Chem. Phys. Lett. 327 (2000) 85–90.

[19] S. Prasad, H.-T. Kwak, T. Clark, P.J. Grandinetti, A simple technique for determining nuclear quadrupole coupling constants with RAPT solid-state NMR spectroscopy, J. Am. Chem. Soc. 124 (2002) 4964–4965.

[20] H.-T. Kwak, S. Prasad, T. Clark, P.J. Grandinetti, Enhancing sensitivity of quadrupolar nuclei in solid-state NMR with multiple rotor assisted population transfers, Solid State Nucl. Magn. Reson. 24 (2003) 71–77.

[21] P.K. Madhu, K.J. Pike, R. Dupree, M.H. Levitt, M.E. Smith, Modulation-aided signal enhancement in the magic angle spinning NMR of spin-5/2 nuclei, Chem. Phys. Lett. 367 (2003) 150–156.

[22] T. Bräuniger, K. Ramaswamy, P.K. Madhu, Enhancement of the central-transition signal in static and magic-angle-spinning NMR of quadrupolar nuclei by frequency-swept fast amplitude-modulated pulses, Chem. Phys. Lett. 383 (2004) 403–410.

[23] T. Bräuniger, P.K. Madhu, A. Pampel, D. Reichert, Application of fast amplitude-modulated pulse trains for signal enhancement in static and magic-angle-spinning ^{47,49}Ti-NMR spectra, Solid State Nucl. Magn. Reson. 26 (2004) 114–120.

[24] Pulse programs for VARIAN INOVA and a FORTRAN90 based calculation tool may be downloaded from: <http://www.physik.uni-halle.de/nmr/dir_tb/swfam.html/>.

[25] R.W. Schurko, I. Hung, C.M. Widdifield, Signal enhancement in NMR spectra of half-integer quadrupolar nuclei via DFS-QCMPG and RAPT-QCMPG pulse sequences, Chem. Phys. Lett. 379 (2003) 1–10.

[26] B. Filsinger, P. Gutsche, U. Haeberlen, N. Weiden, Search for a magnetic-field dependence of the interaction of the nuclear quadrupole moment with the electric-field gradient, J. Magn. Reson. 125 (1997) 280–290.

[27] R.W. Schurko, R.E. Wasylishen, H. Foerster, Characterization of anisotropic aluminum magnetic shielding tensors. Distorted octahedral complexes and linear molecules, J. Phys. Chem. A 102 (1998) 9750–9760.
[28] D. Müller, W. Gessner, A.-R. Grimmer, Bestimmung der Koordinationszahl des Aluminiums in festen Aluminaten aus der chemischen ^{27}Al-Verschiebung, Z. Chem. 17 (1977) 453–454.
[29] M. Bak, J.T. Rasmussen, N.C. Nielsen, SIMPSON: a general simulation program for solid-state NMR spectroscopy, J. Magn. Reson. 147 (2000) 296–330.
[30] S.K. Zaremba, Good lattice points, discrepancy, and numerical integration, Ann. Mat. Pura. Appl. 4 (73) (1966) 293–317.
[31] H. Conroy, Molecular Schrödinger equation. VIII. A new method for the evaluation of multidimensional integrals, J. Chem. Phys. 47 (1967) 5307–5318.
[32] V.B. Cheng, H.H. Suzukawa Jr., M. Wolfsberg, Investigations of a nonrandom numerical method for multidimensional integration, J. Chem. Phys. 59 (1973) 3992–3999.
[33] E. Kupce, R. Freeman, Optimized adiabatic pulses for wideband spin inversion, J. Magn. Reson. A 118 (1996) 299–303.
[34] R. Siegel, T.T. Nakashima, R.E. Wasylishen, Sensitivity enhancement of solid-state NMR spectra of half-integer spin quadrupolar nuclei using hyperbolic secant pulses: applications to spin-5/2 nuclei, Chem. Phys. Lett. 421 (2006) 529–533.